# Energy expressions and free vibration analysis of a rotating double tapered Timoshenko beam featuring bending–torsion coupling

Ozge Ozdemir Ozgumus, Metin O. Kaya *

*Istanbul Technical University, Faculty of Aeronautics and Astronautics, 34469 Maslak, Istanbul, Turkey*

## Abstract

In this study, free vibration analysis of a rotating, double tapered Timoshenko beam featuring coupling between flap-wise bending and torsional vibrations is performed. At the beginning of the study, kinetic and potential energy expressions of a rotating Timoshenko beam having single cross-sectional symmetry are derived in a detailed way by using several explanatory tables and figures. In the following section, Hamilton's principle is applied to the derived energy expressions to obtain the governing differential equations of motion. The parameters for the hub radius, rotational speed, rotary inertia, shear deformation, slenderness ratio, bending–torsion coupling and taper ratio are incorporated into the equations of motion. In the solution part, an efficient mathematical technique, called the differential transform method (DTM), is used to solve the governing differential equations of motion. Using the computer package, Mathematica, the mode shapes are plotted, the effects of the incorporated parameters on the natural frequencies are investigated. The calculated results are tabulated in several tables and plotted in several graphics.
© 2007 Elsevier Ltd. All rights reserved.

*Keywords:* Nonuniform Timoshenko beam; Tapered Timoshenko beam; Rotating Timoshenko beam; Bending–torsion coupled beam; Differential transform method; Differential transformation

## 1. Introduction

When the cross-sections of an isotropic and homogeneous beam have two symmetry axes, the shear center and the centroid are coincident. As a result, bending vibrations are not coupled with the torsional vibration. However, when the cross-sections have only one symmetry axis, the shear center and the centroid do not coincide and the bending vibration that occurs in the plane perpendicular to the symmetry axis is coupled with the torsional vibration.

---

\* Corresponding author. Tel.: +90 212 2853110; fax: +90 212 2853139.
*E-mail address:* kayam@itu.edu.tr (M.O. Kaya).

**Nomenclature**

| | |
|---|---|
| $A$ | cross-sectional area |
| $b_0$ | beam breadth at the root section |
| $c_b$ | breadth taper ratio |
| $c_h$ | height taper ratio |
| $e$ | distance between the centroid of the cross-section and the elastic axis |
| $E$ | Young's modulus |
| $G$ | shear modulus |
| $GJ$ | torsional rigidity |
| $h_0$ | beam height at the root section |
| $\vec{i}, \vec{j}, \vec{k}$ | unit vectors in the $x$, $y$ and $z$ directions |
| $I_y$ | Second moment of inertia about the $y$-axis |
| $I_\alpha$ | mass moment of inertia per unit length about the elastic axis |
| $J$ | torsional rigidity constant |
| $k$ | shear correction factor |
| $kAG$ | shear rigidity |
| $L$ | beam length |
| $P$ | reference point after deformation |
| $P_0$ | reference point before deformation |
| $r$ | inverse of the slenderness ratio $S$ |
| $\vec{r}_0$ | position vector of point $P_0$ |
| $\vec{r}_1$ | position vector of point $P$ |
| $R$ | hub radius |
| $S$ | slenderness ratio |
| $t$ | time |
| $T(x)$ | centrifugal force |
| $\widetilde{T}$ | dimensionless centrifugal force |
| $u_0$ | axial displacement due to the centrifugal force, $T(x)$ |
| $U_{bt}$ | bending–torsion potential energy |
| $U_s$ | shear potential energy |
| $V_x, V_y, V_z$ | velocity components of point $P$ |
| $W[k], \varphi[k], \psi[k]$ | transformed functions |
| $w$ | flapwise bending displacement |
| $x$ | longitudinal coordinate |
| $\bar{x}$ | longitudinal coordinate parameter |
| $x_0, y_0, z_0$ | coordinates of point $P_0$ |
| $x_1, y_1, z_1$ | coordinates of point $P$ |
| $\delta$ | hub radius parameter |
| $\delta W$ | virtual work of the nonconservative forces |
| $\gamma$ | shear angle |
| $\varepsilon_0$ | uniform strain due to the centrifugal force, $T(x)$ |
| $\varepsilon_{ij}$ | classical strain tensor |
| $\varepsilon_{xx}$ | axial strain |
| $\varepsilon_{\eta\eta}, \varepsilon_{\xi\xi}$ | transverse normal strains |
| $\eta$ | sectional coordinate of $P_0$ corresponding to major principal axis on the elastic axis |
| $\mu$ | natural frequency parameter |
| $\xi$ | sectional coordinate of $P_0$ normal to $\eta$-axis |
| $\rho$ | density of the beam material |
| $\rho A$ | mass per unit length |

| $\psi$ | torsion angle |
|---|---|
| $\varphi$ | rotation angle due to bending |
| $\omega$ | circular natural frequency |
| $\Omega$ | constant rotational speed |
| $\overline{\Omega}$ | rotational speed parameter |

Several engineering components, such as blades in turbines, compressors, propellers or helicopter rotors, usually have non-coincident elastic and inertial axes, which are respectively the shear centers and the loci of centroids of the cross-sections. Therefore, the determination of the dynamic characteristics of rotating coupled beams is of great importance in the design of such components. As a result, free and forced vibration characteristics of bending–torsion coupled beams have been an interesting area for many researchers. Houbolt and Brooks [1] derived the equations of motion of a cantilever Euler–Bernoulli beam in coupled bending–bending–torsion vibration motion by including the rotation effects. Bishop and Price [2] studied the coupled bending–torsion vibration of the Timoshenko beams without including the warping stiffness. Subrahmanyam et al. [3] presented natural frequencies and modal shapes of a rotating blade of asymmetrical aerofoil cross-section with allowance for shear deflection and rotary inertia. Hallauer and Liu [4] and Friberg [5] derived the exact dynamic stiffness matrix for a bending–torsion coupled Euler–Bernoulli beam with the warping stiffness ignored. Dokumaci [6] derived the exact analytical expressions for the solution of the bending–torsion equations without the warping effect. Bishop et al. [7], extended the study of Dokumaci by including the warping effect. Karadag [8,9] investigated the dynamic characteristics of rotating and nonrotating practical bladed discs by taking blade shear center effects into account. Banerjee and Williams [10,11] derived the analytical expressions for the coupled bending–torsion dynamic stiffness matrix of a Timoshenko beam excluding the warping stiffness effect. Banerjee et al. [12] recast the study of Bishop et al. [7], by using the dynamic stiffness matrix. Eslimy-Isfahany et al. [13] studied the response of a bending–torsion coupled beam to deterministic and random loads. Bercin and Tanaka [14], included the effects of warping, shear deformation and rotary inertia in their study of coupled flexural–torsional vibrations of beams having single axis of symmetry. Hashemi and Richard [15] presented a new dynamic finite element for the bending–torsion coupled Euler–Bernoulli beams with the warping stiffness omitted. Sabuncu and Evran [16,17], studied the dynamic stability of an asymmetric cross-section rotating Timoshenko beam with and without pretwist.

In this study, which is an extension of the authors' previous works [18–22], free vibration analysis of a double tapered, rotating, cantilever Timoshenko beam featuring coupling between flapwise bending and torsional vibrations is performed. At the beginning of the study, expressions for both the kinetic and the potential energies are derived in a detailed way by using explanatory tables and figures. In the next step, the governing differential equations of motion are obtained applying the Hamilton's principle. In the solution part, the equations of motion, including the parameters for the hub radius, rotational speed, rotary inertia, shear deformation, slenderness ratio, bending–torsion coupling and taper ratios, are solved using an efficient mathematical technique, called the differential transform method (DTM). Finally, using the computer package, Mathematica, the natural frequencies are calculated, the mode shapes are plotted and effects of the parameters, mentioned above, are investigated. Unfortunately, a suitable example that studies the rotating, double tapered, coupled Timoshenko beam model has not been solved by any of the studies in open literature so far. Therefore, this beam is modeled in the finite element program, ABAQUS in order to validate the calculated results of this study. Additionally, some examples that study simpler Timoshenko beam models are found in open literature and solved in order to make comparisons. Consequently, it is observed that there is a good agreement between the results.

Partial differential equations are often used to describe engineering problems whose closed form solutions are very difficult to establish in many cases. Therefore, approximate numerical methods, i.e. finite element, finite difference, boundary element methods, etc. are often preferred. However, in spite of the advantages of these on hand methods and the computer codes that are based on them, closed form solutions are more attractive due to their implementation of the physics of the problem and their convenience for parametric studies. Moreover, closed form solutions have the capability and facility to solve inverse problem of determining

and designing the geometry and characteristics of an engineering system and to achieve a prescribed behaviour of the system. Considering the advantages of the closed form solutions mentioned above, the differential transform method is introduced in this study as the solution method. DTM was first introduced by Zhou [23] to solve both linear and nonlinear initial value problems in electric circuit analysis. The method can deal with nonlinear problems so Chiou and Tzeng [24] applied the Taylor transform to solve nonlinear vibration problems. Additionally, the method may be used to solve both ordinary and partial differential equations. Thus, Jang et al. [25] applied the two-dimensional differential transform method to the solution of partial differential equations. Abdel and Hassan [26] adopted the differential transform method to solve some eigenvalue problems. Since previous studies have shown this method to be an efficient tool, in recent years it has been applied to solve boundary value problems for integro-differential equations [27], differential–difference equations [28], aeroelasticity problems [29,30], and many other linear–nonlinear problems which are very important in modelling many phenomena in viscoelasticity, fluid mechanics, biology, chemistry, acoustics, control theory, etc. Besides the variety of the problems to which DTM may be applied, its simplicity and accuracy in calculating the natural frequencies and plotting the mode shapes makes this method outstanding among many other methods.

## 2. Beam configuration

The governing differential equations of motion are derived for the bending–torsion coupled free vibration of a rotating, double tapered, cantilever Timoshenko beam represented by Fig. 1. Here, a cantilever beam of length $L$, which is fixed at point O to a rigid hub, is shown. The hub has the radius $R$ and rotates at a constant rotational speed, $\Omega$. The beam tapers linearly from a height $h_0$ at the root to $h$ at the free end in the $xz$ plane and from a breadth $b_0$ to $b$ in the $xy$ plane. The cross-sectional view and the associated dimensions at the root section ($b_0 = 30$ cm, $h_0 = 10$ cm) are introduced in Fig. 2a. The side and the top views of the beam are shown in Fig. 2b and c, respectively. As it is seen in Fig. 2a, the cross-section of the beam is symmetric only about one axis, the $y$-axis. Therefore as mentioned in the Section 1, the mass and elastic axes of the beam, which are respectively the loci of centroids and shear centers of the cross-sections, are separated by a distance $e$, as shown in Fig. 1 and the flapwise bending vibration is coupled with the torsional vibration.
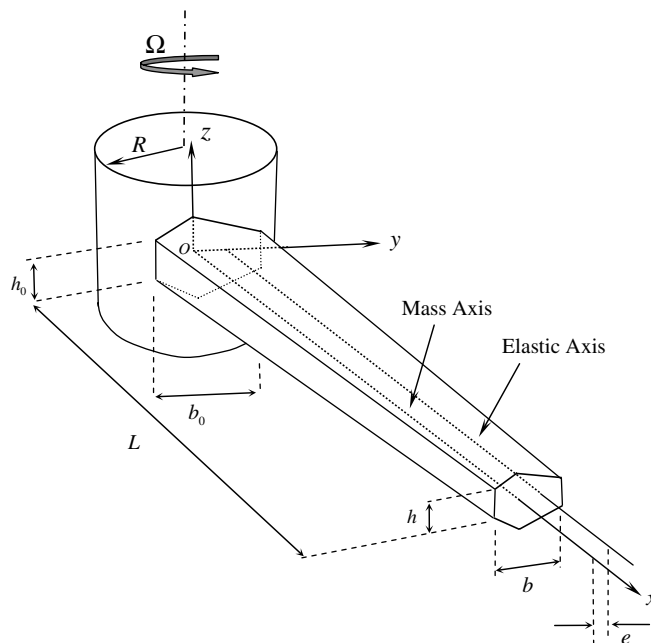


Fig. 1. Configuration of a double tapered, rotating, cantilever Timoshenko beam featuring bending–torsion coupling.
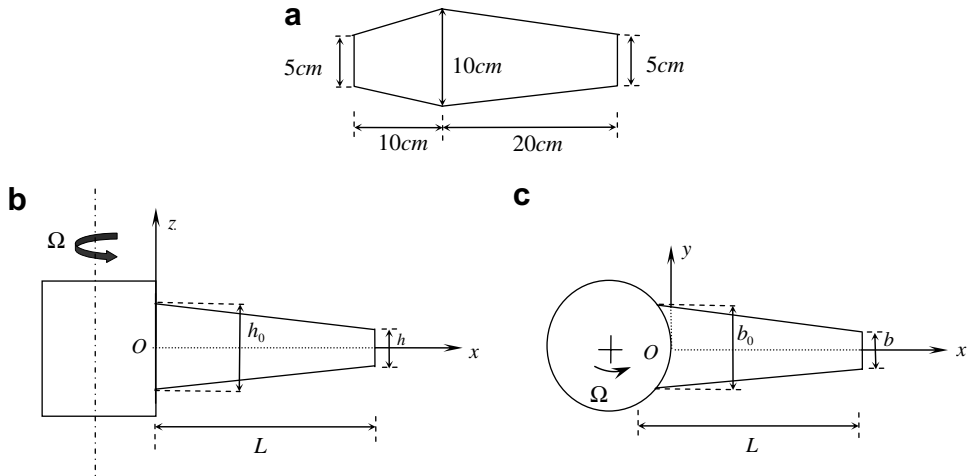
Fig. 2. (a) Cross-sectional view, (b) side view and (c) top view of the double tapered Timoshenko beam with cross-section having one symmetry axis.

The following assumptions are made in this study,

(a) The flapwise bending displacement and the torsion angle of the beam are small.
(b) The planar cross-sections that are initially perpendicular to the neutral axis of the beam remain plane, but no longer perpendicular to the neutral axis during bending.
(c) The beam material is homogeneous and isotropic.

## 3. Derivation of the equations of motion

The cross-sectional and the side views of the bending–torsion deflections of a rotating uniform Timoshenko beam are given in Fig. 3a and b, respectively. Here, the chosen reference point is represented by $P_0$ before deformation and by $P$ after deformation.
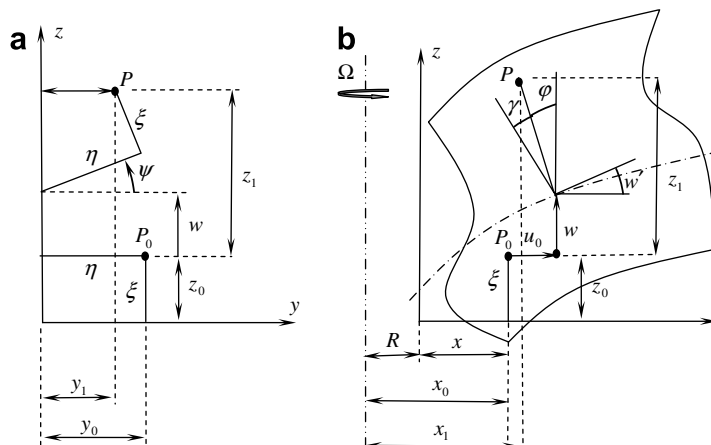


Fig. 3. (a) Cross-sectional view and (b) side view of the bending–torsion deflections of the reference point.

### 3.1. Derivation of the potential energy expression

When Fig. 3a and b are considered, the coordinates of the reference point can be written as follows:

(a) Before deformation (coordinates of $P_0$):

$$x_0 = R + x \tag{1a}$$
$$y_0 = \eta \tag{1b}$$
$$z_0 = \xi \tag{1c}$$

(b) After deformation (coordinates of $P$):

$$x_1 = R + x + u_0 - (\xi \cos\psi + \eta \sin\psi) \sin\varphi \tag{2a}$$
$$y_1 = \eta \cos\psi - \xi \sin\psi \tag{2b}$$
$$z_1 = w + \xi \cos\psi + \eta \sin\psi \tag{2c}$$

where $x$ is the longitudinal coordinate, $u_0$ is the axial displacement due to the centrifugal force, $\eta$ and $\xi$ are the sectional coordinates of $P_0$, $w$ is the flapwise bending displacement, $\varphi$ is the rotation due to bending, $\gamma$ is the shear angle and $\psi$ is the torsion angle. The rotation due to bending, $\varphi$, is small so it is assumed that $\sin\varphi \cong \varphi$. The torsion angle, $\psi$, is also small so $\sin\psi \cong \psi$, but in order to investigate the torsional stability, the second order terms of $\cos\psi$ are kept so it is assumed that $\cos\psi \cong 1 - \frac{\psi^2}{2}$. Using these assumptions, Eqs. (2a)–(2c) can be rewritten as follows:

$$x_1 = R + x + u_0 - \left[\xi\left(1 - \frac{\psi^2}{2}\right) + \eta\psi\right]\varphi \tag{3a}$$

$$y_1 = \eta\left(1 - \frac{\psi^2}{2}\right) - \xi\psi \tag{3b}$$

$$z_1 = w + \xi\left(1 - \frac{\psi^2}{2}\right) + \eta\psi \tag{3c}$$

Knowing that $\vec{r}_0$ and $\vec{r}_1$ are the position vectors of the reference point before and after deformation, respectively, $\vec{dr_0}$ and $\vec{dr_1}$ can be given by

$$\vec{dr_0} = (dx_0)\vec{i} + (dy_0)\vec{j} + (dz_0)\vec{k} \tag{4a}$$
$$\vec{dr_1} = (dx_1)\vec{i} + (dy_1)\vec{j} + (dz_1)\vec{k} \tag{4b}$$

where $\vec{i}$, $\vec{j}$ and $\vec{k}$ are the unit vectors in the $x$, $y$ and $z$ directions, respectively.

The components of $dr_0$ and $dr_1$ are expressed as follows:

$$dx_0 = dx \tag{5a}$$
$$dy_0 = d\eta \tag{5b}$$
$$dz_0 = d\xi \tag{5c}$$

$$dx_1 = \left\{1 + u_0' - \left[\xi\left(1 - \frac{\psi^2}{2}\right) + \eta\psi\right]\varphi' + (\xi\psi\psi' - \eta\psi')\varphi\right\}dx - \psi\varphi\,d\eta - \left(1 - \frac{\psi^2}{2}\right)\varphi\,d\xi \tag{6a}$$

$$dy_1 = -(\eta\psi\psi' + \xi\psi')dx + \left(1 - \frac{\psi^2}{2}\right)d\eta - \psi\,d\xi \tag{6b}$$

$$dz_1 = (w' - \xi\psi\psi' + \eta\psi')dx + \psi\,d\eta + \left(1 - \frac{\psi^2}{2}\right)d\xi \tag{6c}$$

The classical strain tensor $\varepsilon_{ij}$ may be obtained using the equilibrium equation below [31]:

$$\vec{dr_1} \cdot \vec{dr_1} - \vec{dr_0} \cdot \vec{dr_0} = 2[\,dx \quad d\eta \quad d\xi\,][\varepsilon_{ij}]\begin{Bmatrix} dx \\ d\eta \\ d\xi \end{Bmatrix} \tag{7}$$

where $[\varepsilon_{ij}] = \begin{bmatrix} \varepsilon_{xx} & \varepsilon_{x\eta} & \varepsilon_{x\xi} \\ \varepsilon_{\eta x} & \varepsilon_{\eta\eta} & \varepsilon_{\eta\xi} \\ \varepsilon_{\xi x} & \varepsilon_{\xi\eta} & \varepsilon_{\xi\xi} \end{bmatrix}$.

Substituting Eqs. (5a)–(6c) into Eq. (7), the elements of the strain tensor $\varepsilon_{ij}$ are obtained as follows:

$$2\gamma_{xx} = \left\{ 1 + u_0' - \left[ \xi\left(1 - \frac{\psi^2}{2}\right) + \eta\psi \right]\varphi' + (\xi\psi\psi' - \eta\psi')\varphi \right\}^2$$
$$+ (\eta\psi\psi' + \xi\psi')^2 + (w' - \xi\psi\psi' + \psi'\eta)^2 - 1 \tag{8a}$$

$$2\gamma_{x\eta} = -\left\{ 1 + u_0' - \left[ \xi\left(1 - \frac{\psi^2}{2}\right) + \eta\psi \right]\varphi' + (\xi\psi\psi' - \eta\psi')\varphi \right\}(\psi\varphi)$$
$$- (\eta\psi\psi' + \xi\psi')\left(1 - \frac{\psi^2}{2}\right) + (w' - \xi\psi\psi' + \eta\psi')\psi \tag{8b}$$

$$2\gamma_{x\xi} = -\left\{ 1 + u_0' - \left[ \xi\left(1 - \frac{\psi^2}{2}\right) + \eta\psi \right]\varphi' + (\xi\psi\psi' - \eta\psi')\varphi \right\}\left(1 - \frac{\psi^2}{2}\right)\varphi$$
$$+ (\eta\psi\psi' + \xi\psi')\psi + (w' - \xi\psi\psi' + \eta\psi')\left(1 - \frac{\psi^2}{2}\right) \tag{8c}$$

In this study $\gamma_{xx}$, $\gamma_{x\eta}$ and $\gamma_{x\xi}$ are used in the calculations because as noted by Hodges and Dowell [32], for long slender beams, the axial strain $\varepsilon_{xx}$ is dominant over the transverse normal strains, $\varepsilon_{\eta\eta}$ and $\varepsilon_{\xi\xi}$. Additionally, the shear strain $\varepsilon_{\eta\xi}$ is two order smaller than the other shear strains, $\varepsilon_{x\eta}$ and $\varepsilon_{x\xi}$.

In order to obtain simpler expressions for the strain components, higher order terms must be neglected so an order of magnitude analysis is performed by using the ordering scheme, taken from Hodges and Dowell [32] and introduced in Table A1 in the Appendix A. The Euler–Bernoulli Beam Theory is used by Hodges and Dowell [32] and in the present study, their formulation is modified for a Timoshenko beam and a new expression, $\gamma = w' - \varphi = O(\varepsilon^2)$, is added to their ordering scheme as a contribution to the literature. Using Table A1 and Eqs. (8a)–(8c), the following simplified strain expressions are obtained:

$$\varepsilon_{xx} = u_0' - \xi\varphi' + \frac{1}{2}(w')^2 + \frac{1}{2}(\eta^2 + \xi^2)(\psi')^2 \tag{9a}$$

$$\gamma_{x\eta} = -\xi\psi' \tag{9b}$$

$$\gamma_{x\xi} = w' - \varphi + \eta\psi' \tag{9c}$$

The expression for the bending–torsion potential energy, $U_{bt}$, is given by

$$U_{bt} = \frac{1}{2}\int_0^L \left( \int\int_A E\varepsilon_{xx}^2\,d\eta\,d\xi \right)dx \tag{10}$$

where $A$ is the cross-sectional area and $E$ is the Young's modulus.

Substituting Eq. (9a) into Eq. (10), the following expression is obtained

$$U_{bt} = \frac{1}{2}\int_0^L \left( \int\int_A E\left\{ u_0' - \xi\varphi' + \frac{1}{2}(w')^2 + \frac{1}{2}(\eta^2 + \xi^2)(\psi')^2 \right\}^2 d\eta\,d\xi \right)dx \tag{11}$$

Taking integration over the blade cross-section and referring to the definitions given by Table A2 in the Appendix A, the following potential energy expression is obtained for bending–torsion

$$U_{\text{bt}} = \frac{1}{2}\int_0^L EA(u_0')^2 \mathrm{d}x + \frac{1}{2}\int_0^L EI_y(\varphi')^2 \mathrm{d}x + \frac{1}{2}\int_0^L EAu_0'(w')^2 \mathrm{d}x + \frac{1}{2}\int_0^L I_\alpha \frac{u_0'}{\rho}(\psi')^2 \mathrm{d}x \tag{12}$$

where $I_\alpha$ is the mass moment of inertia per unit length about the elastic axis and $I_y$ is the second moment of inertia about the $y$-axis.

The uniform strain $\varepsilon_0$ and the associated axial displacement $u_0$ due to the centrifugal force $T(x)$ is given by

$$u_0'(x) = \varepsilon_0(x) = \frac{T(x)}{EA} \tag{13}$$

where the centrifugal force is expressed as follows:

$$T(x) = \int_x^L \rho A \Omega^2 (R + x) \mathrm{d}x \tag{14}$$

where $\rho A$ is the mass per unit length.

Substituting Eqs. (13) and (14) into Eq. (12) and noting that the $\frac{1}{2}\int_0^L \frac{T^2(x)}{EA}\mathrm{d}x$ term is constant and will be denoted by $C_1$, the final form of the bending–torsion potential energy is obtained as follows:

$$U_{\text{bt}} = \frac{1}{2}\int_0^L EI_y(\varphi')^2 \mathrm{d}x + \frac{1}{2}\int_0^L T\left[(w')^2 + \frac{I_\alpha}{\rho A}(\psi')^2\right]\mathrm{d}x + C_1 \tag{15}$$

The expression for the shear potential energy, $U_s$, is given by

$$U_s = \frac{1}{2}\int_0^L \left(\iint_A G\left(\gamma_{x\eta}^2 + \gamma_{x\xi}^2\right)\mathrm{d}\eta\,\mathrm{d}\xi\right)\mathrm{d}x \tag{16}$$

where $G$ is the shear modulus.

Substituting Eqs. (9b) and (9c) into Eq. (16), the following expression is obtained for the shear potential energy

$$U_s = \frac{1}{2}\int_0^L \left(\iint_A G\left[\xi^2(\psi')^2 + (w' - \varphi + \eta\psi')^2\right]\mathrm{d}\eta\,\mathrm{d}\xi\right)\mathrm{d}x \tag{17}$$

Referring to the definitions given by Table A2, Eq. (17) can be rewritten as follows:

$$U_s = \frac{1}{2}\int_0^L \{kAG(w' - \varphi)^2 \mathrm{d}x + GJ(\psi')^2\}\mathrm{d}x \tag{18}$$

where $k$ is the shear correction factor, $kAG$ is the shear rigidity and $GJ$ is the torsional rigidity of the beam cross-section.

Summing Eqs. (15) and (18), the total potential energy expression is given by

$$U = \frac{1}{2}\left[\int_0^L \left\{EI_y(\varphi')^2 + T\left[(w')^2 + \frac{I_\alpha}{\rho A}(\psi')^2\right] + kAG(w' - \varphi)^2 + GJ(\psi')^2 + C_1\right\}\mathrm{d}x\right] \tag{19}$$

### 3.2. Derivation of the kinetic energy expression

The velocity vector of point $P$ is expressed as follows:

$$\vec{V} = \frac{\partial \vec{r}}{\partial t} + \Omega\vec{k} \times \vec{r} \tag{20}$$

where

$$\vec{r} = x_1\vec{i} + y_1\vec{j} + z_1\vec{k} \tag{21}$$

Substituting Eq. (21) into Eq. (20), the velocity vector expression can be given by

$$\vec{V} = (\dot{x}_1 - \Omega y_1)\vec{i} + (\dot{y}_1 + \Omega x_1)\vec{j} + \dot{z}_1\vec{k} \tag{22}$$

where $\dot{x}$, $\dot{y}$ and $\dot{z}$ are the derivatives of the coordinates with respect to time, $t$.

Substituting Eqs. (3a)–(3c) into Eq. (22) and applying the ordering scheme given by Table A1, the velocity components are obtained as follows:

$$V_x = -\left[\xi\left(1 - \frac{\psi^2}{2}\right) + \eta\psi\right]\dot{\varphi} + (\xi\psi\dot{\psi} - \eta\dot{\psi})\varphi - \left[\eta\left(1 - \frac{\psi^2}{2}\right) - \xi\psi\right]\Omega \tag{23a}$$

$$V_y = -(\eta\psi + \xi)\dot{\psi} + \left\{R + x + u_0 - \left[\xi\left(1 - \frac{\psi^2}{2}\right) + \eta\psi\right]\varphi\right\}\Omega \tag{23b}$$

$$V_z = \dot{w} + (\eta - \xi\psi)\dot{\psi} \tag{23c}$$

The kinetic energy expression is given by

$$\Im = \frac{1}{2}\int_0^L \left(\iint_A \rho\left(V_x^2 + V_y^2 + V_z^2\right)\mathrm{d}\eta\,\mathrm{d}\xi\right)\mathrm{d}x \tag{24}$$

Substituting Eqs. (23a)–(23c) into Eq. (24) and referring to the definitions given by Table A3 in Appendix A, the following kinetic energy expression is obtained.

$$\Im = \frac{1}{2}\int_0^L \left\{\rho A\dot{w}^2 + \rho I_y\left[\Omega^2\varphi^2 + \dot{\varphi}^2 + 2\Omega(\varphi\dot{\psi} - \dot{\varphi}\psi)\right] + I_\alpha\dot{\psi}^2 + \rho(I_y - I_z)\Omega^2\psi^2\right.$$
$$\left. + 2\rho I_z\Omega(\varphi\dot{\psi} + \dot{\varphi}\psi) + 2\rho Ae\left[\dot{w}\dot{\psi} - (R+x)\Omega^2\psi\varphi\right]\right\}\mathrm{d}x \tag{25}$$

### 3.3. Governing differential equations of motion

The governing differential equations of motion and the associated boundary conditions are obtained by applying the Hamilton's principle, given below, to Eqs. (19) and (25):

$$\int_{t_1}^{t_2}\delta(U - \Im - W)\mathrm{d}t = 0 \tag{26}$$

In this study, undamped, free vibration analysis is performed so variation of the virtual work done by the non-conservative forces, $\delta W$, in Eq. (26) is zero. Therefore, variation of the kinetic and potential energy expressions are taken and substituted into Eq. (26).

Using variational principles, the differential equations of motions for a rotating, nonuniform Timoshenko beam with bending–torsion coupling are derived as follows:

$$\rho A\frac{\partial^2 w}{\partial t^2} + \rho Ae\frac{\partial^2 \psi}{\partial t^2} - \frac{\partial}{\partial x}\left(T\frac{\partial w}{\partial x}\right) - \frac{\partial}{\partial x}\left[kAG\left(\frac{\partial w}{\partial x} - \varphi\right)\right] = 0 \tag{27a}$$

$$\rho I_y\frac{\partial^2 \varphi}{\partial t^2} - \rho I_y\Omega^2\varphi - \frac{\partial}{\partial x}\left(EI_y\frac{\partial \varphi}{\partial x}\right) - kAG\left(\frac{\partial w}{\partial x} - \varphi\right) - 2\rho I_y\Omega\frac{\partial \psi}{\partial t} + \rho Ae\Omega^2(R+x)\psi = 0 \tag{27b}$$

$$I_\alpha\frac{\partial^2 \psi}{\partial t^2} + \rho Ae\frac{\partial^2 w}{\partial t^2} - \rho(I_y - I_z)\Omega^2\psi - \frac{\partial}{\partial x}\left(GJ\frac{\partial \psi}{\partial x}\right) - \frac{\partial}{\partial x}\left(\frac{TI_\alpha}{\rho A}\frac{\partial \psi}{\partial x}\right) + 2\rho I_y\Omega\frac{\partial \varphi}{\partial t} + \rho Ae\Omega^2(R+x)\varphi = 0 \tag{27c}$$

Neglecting the Coriolis terms, Eqs. (27a)–(27c) reduce to the following equations:

$$\rho A\frac{\partial^2 w}{\partial t^2} + \rho Ae\frac{\partial^2 \psi}{\partial t^2} - \frac{\partial}{\partial x}\left(T\frac{\partial w}{\partial x}\right) - \frac{\partial}{\partial x}\left[kAG\left(\frac{\partial w}{\partial x} - \varphi\right)\right] = 0 \tag{28a}$$

$$\rho I_y\frac{\partial^2 \varphi}{\partial t^2} - \rho I_y\Omega^2\varphi - \frac{\partial}{\partial x}\left(EI_y\frac{\partial \varphi}{\partial x}\right) - kAG\left(\frac{\partial w}{\partial x} - \varphi\right) + \rho Ae\Omega^2(R+x)\psi = 0 \tag{28b}$$

$$I_\alpha\frac{\partial^2 \psi}{\partial t^2} + \rho Ae\frac{\partial^2 w}{\partial t^2} - \rho(I_y - I_z)\Omega^2\psi - \frac{\partial}{\partial x}\left(GJ\frac{\partial \psi}{\partial x}\right) - \frac{\partial}{\partial x}\left(\frac{TI_\alpha}{\rho A}\frac{\partial \psi}{\partial x}\right) + \rho Ae\Omega^2(R+x)\varphi = 0 \tag{28c}$$

Here, $w$ is the flapwise bending displacement, $\varphi$ is the rotation due to bending and $\psi$ is the torsion angle.

The term, $\rho I_y \Omega^2 \varphi$, which appears in Eq. (28b) as a result of our derivations, can be important when the constant rotational speed, $\Omega$, is high. However, it is not taken into account by some authors [33,34]. The physical description of this term is that as a result of the bending deformation, the elements that are symmetrically placed with respect to the mid-plane of the beam cross-section have different radii which makes these elements experience different centrifugal force values although the net centrifugal force is independent of the sectional rotation. Thus, a moment that has the value of $\rho I_y \Omega^2 \varphi$ appears [35].

Additionally, after the application of the Hamilton's principle, the boundary conditions are obtained as follows:

- The geometric boundary conditions at the cantilever end, $x = 0$, of the Timoshenko beam,

$$w(0,t) = \varphi(0,t) = \psi(0,t) = 0 \tag{29a}$$

- The natural boundary conditions at the free end, $x = L$, of the Timoshenko beam,

Shear force: $Tw' + kAG(w' - \varphi) = 0$     (29b)
Bending moment: $EI_y \varphi' = 0$     (29c)
Torsion: $GJ\psi' = 0$     (29d)

The boundary conditions expressed by Eqs. (29b)–(29d) can be written in a simpler form by noting that the centrifugal force is zero at the free end of the beam, $T(L) = 0$.

$$w' - \varphi = 0 \tag{30a}$$
$$\varphi' = 0 \tag{30b}$$
$$\psi' = 0 \tag{30c}$$

## 4. Vibration analysis

### 4.1. Harmonic motion assumption

In order to investigate the undamped free vibration of the beam model considered in this study, a sinusoidal variation of $w(x,t)$, $\psi(x,t)$ and $\varphi(x,t)$ with a circular natural frequency, $\omega$, is assumed and the functions are approximated as

$$w(x,t) = \bar{w}(x)e^{i\omega t} \tag{31a}$$
$$\psi(x,t) = \bar{\psi}(x)e^{i\omega t} \tag{31b}$$
$$\varphi(x,t) = \bar{\varphi}(x)e^{i\omega t} \tag{31c}$$

where $\bar{w}(x)$, $\bar{\psi}(x)$ and $\bar{\varphi}(x)$ are the amplitudes of the sinusoidally varying flapwise bending displacement, angle due to bending and torsional rotation.

Substituting Eqs. (31a)–(31c) into Eqs. (28a)–(28c) results in the following equations of motion.

$$\omega^2 \rho A \bar{w} + \omega^2 \rho A e \bar{\psi} + (T\bar{w}')' + [kAG(\bar{w}' - \bar{\varphi})]' = 0 \tag{32a}$$

$$\rho I_y \omega^2 \bar{\varphi} + \rho I_y \Omega^2 \bar{\varphi} + (EI_y \bar{\varphi}')' + kAG(\bar{w}' - \bar{\varphi}) - \rho A e \Omega^2 (R+x)\bar{\psi} = 0 \tag{32b}$$

$$\omega^2 I_\alpha \bar{\psi} + \omega^2 \rho A e \bar{w} + \rho(I_y - I_z)\Omega^2 \bar{\psi} + (GJ\bar{\psi}')' + \left(T\frac{I_\alpha}{\rho A}\bar{\psi}'\right)' - \rho A e \Omega^2 (R+x)\bar{\varphi} = 0 \tag{32c}$$

where primes mean differentiation with respect to the longitudinal coordinate, $x$.

### 4.2. Tapered beam assumptions and dimensionless parameters

In this study, the beam model tapers linearly in the $xz$ and the $xy$ planes with respect to the taper ratios, $c_h$ and $c_b$, respectively. Considering this tapered beam model, given in Figs. 1 and 2, the following assumptions are made

$$b = b_0\left(1 - c_b\frac{x}{L}\right) \tag{33a}$$

$$h = h_0\left(1 - c_h\frac{x}{L}\right) \tag{33b}$$

$$e = e_0\left(1 - c_b\frac{x}{L}\right) \tag{33c}$$

$$A = A_0\left(1 - c_b\frac{x}{L}\right)\left(1 - c_h\frac{x}{L}\right) \tag{33d}$$

$$I_y = I_{y0}\left(1 - c_b\frac{x}{L}\right)\left(1 - c_h\frac{x}{L}\right)^3 \tag{33e}$$

$$J = J_0\left(1 - c_b\frac{x}{L}\right)\left(1 - c_h\frac{x}{L}\right)^3 \tag{33f}$$

$$I_\alpha = I_{\alpha0}\left(1 - c_b\frac{x}{L}\right)\left(1 - c_h\frac{x}{L}\right)^3 \tag{33g}$$

Here, the subscript ( )$_0$ denotes the values at the root section of the tapered beam, $c_b$ and $c_h$ represent the breadth and taper ratios, respectively. These taper ratios can be expressed as follows:

$$c_b = 1 - \frac{b}{b_0} \tag{34a}$$

$$c_h = 1 - \frac{h}{h_0} \tag{34b}$$

In order to make comparisons with the results in open literature, the following dimensionless parameters are introduced:

$$
\begin{aligned}
&\bar{x} = \frac{x}{L} \quad \delta = \frac{R}{L} \quad \overline{\Omega}^2 = \frac{\rho A_0 L^4 \Omega^2}{EI_{y0}} \quad r^2 = \frac{1}{S^2} = \frac{I_{y0}}{A_0 L^2} \quad \mu^2 = \frac{\rho A_0 L^4 \omega^2}{EI_{y0}} \\
&\bar{e} = \frac{e_0}{L} \quad \tilde{w} = \frac{\bar{w}}{L} \quad s^2 = \frac{EI_{y0}}{kA_0 GL^2} \quad \sigma^2 = \frac{GJ_0}{EI_{y0}} \quad r_\alpha^2 = \frac{I_{\alpha0}}{\rho A_0 L^2}
\end{aligned} \tag{35}
$$

Here, $\delta$ is the hub radius parameter, $\overline{\Omega}$ is the rotational speed parameter, $\mu$ is the natural frequency parameter, $r$ is the inverse of the slenderness ratio $S$.

Using the related dimensionless parameters and the tapered beam assumptions, the centrifugal force, given by Eq. (14), can be written in the dimensionless form as follows:

$$
\begin{aligned}
\widetilde{T} = \rho\Omega^2 L^2 \int_{\bar{x}}^1 (\delta + \bar{x})\mathrm{d}\bar{x} = \frac{\rho\Omega^2 L^2 A_0}{12} &\left\{ c_b\left[c_h\left(3 + 4\delta - 4\bar{x}^3\delta - 3\bar{x}^4\right) + 4\bar{x}^3 + 6\bar{x}^2\delta - 4 - 6\delta\right] \right. \\
&\left. + 2(\bar{x} - 1)\left[c_h\left(3\delta(\bar{x} + 1) + 2(\bar{x}^2 + \bar{x} + 1)\right)\right] \right\}
\end{aligned} \tag{36}
$$

where $\widetilde{T}$ represents the dimensionless centrifugal force.

Substituting the dimensionless form of the centrifugal force, the dimensionless parameters and the tapered beam assumptions into Eqs. (32a)–(32c), the dimensionless governing differential equations of motion are obtained:

$$\frac{\mathrm{d}}{\mathrm{d}\bar{x}}\left\{\left[\delta(1-\bar{x})+\frac{1-\delta(c_\mathrm{b}+c_\mathrm{h})}{2}\left(1-\bar{x}^2\right)+\frac{c_\mathrm{b}c_\mathrm{h}\delta-c_\mathrm{b}-c_\mathrm{h}}{3}\left(1-\bar{x}^3\right)+\frac{c_\mathrm{b}c_\mathrm{h}}{4}\left(1-\bar{x}^4\right)\right]\frac{\mathrm{d}\tilde{w}}{\mathrm{d}\bar{x}}\right\}$$

$$+\left(\frac{\mu}{\overline{\Omega}}\right)^2(1-c_\mathrm{b}\bar{x})(1-c_\mathrm{h}\bar{x})\tilde{w}+\bar{e}\left(\frac{\mu}{\overline{\Omega}}\right)^2(1-c_\mathrm{b}\bar{x})^2(1-c_\mathrm{h}\bar{x})\bar{\psi}$$

$$+\left(\frac{1}{s\overline{\Omega}}\right)^2\frac{\mathrm{d}}{\mathrm{d}\bar{x}}\left[(1-c_\mathrm{b}\bar{x})(1-c_\mathrm{h}\bar{x})\left(\frac{\mathrm{d}\tilde{w}}{\mathrm{d}\bar{x}}-\bar{\varphi}\right)\right]=0 \tag{37a}$$

$$\frac{\mathrm{d}}{\mathrm{d}\bar{x}}\left[(1-c_\mathrm{b}\bar{x})(1-c_\mathrm{h}\bar{x})^3\frac{\mathrm{d}\bar{\varphi}}{\mathrm{d}\bar{x}}\right]+r^2(\mu^2+\overline{\Omega}^2)(1-c_\mathrm{b}\bar{x})(1-c_\mathrm{h}\bar{x})^3\bar{\varphi}-\bar{e}\overline{\Omega}^2(\delta+\bar{x})(1-c_\mathrm{b}\bar{x})^2(1-c_\mathrm{h}\bar{x})\bar{\psi}$$

$$+\frac{(1-c_\mathrm{b}\bar{x})(1-c_\mathrm{h}\bar{x})}{s^2}\left(\frac{\mathrm{d}\tilde{w}}{\mathrm{d}\bar{x}}-\bar{\varphi}\right)=0 \tag{37b}$$

$$\frac{\mathrm{d}}{\mathrm{d}\bar{x}}\left\{\left[\delta(1-\bar{x})+\frac{1-\delta(c_\mathrm{b}+c_\mathrm{h})}{2}\left(1-\bar{x}^2\right)+\frac{c_\mathrm{b}c_\mathrm{h}\delta-c_\mathrm{b}-c_\mathrm{h}}{3}\left(1-\bar{x}^3\right)+\frac{c_\mathrm{b}c_\mathrm{h}}{4}\left(1-\bar{x}^4\right)\right](1-c_\mathrm{h}\bar{x})^2\frac{\mathrm{d}\tilde{w}}{\mathrm{d}\bar{x}}\right\}$$

$$+\bar{e}\left(\frac{\mu}{r_\alpha\overline{\Omega}}\right)^2(1-c_\mathrm{b}\bar{x})^2(1-c_\mathrm{h}\bar{x})\tilde{w}-\frac{\bar{e}}{r_\alpha^2}(\delta+\bar{x})(1-c_\mathrm{b}\bar{x})^2(1-c_\mathrm{h}\bar{x})\bar{\varphi}$$

$$+\left[\left(\frac{r}{r_\alpha}\right)^2+\left(\frac{\mu}{\overline{\Omega}}\right)^2\right](1-c_\mathrm{b}\bar{x})(1-c_\mathrm{h}\bar{x})^3\bar{\psi}+\left(\frac{\sigma}{r_\alpha\overline{\Omega}}\right)^2\left[(1-c_\mathrm{b}\bar{x})(1-c_\mathrm{h}\bar{x})^3\frac{\mathrm{d}\bar{\psi}}{\mathrm{d}\bar{x}}\right]=0 \tag{37c}$$

### 4.3. The differential transform method

The differential transform method is a semi-analytic transformation technique based on the Taylor series expansion and is a useful tool to obtain analytical solutions of the differential equations. In this method, certain transformation rules are applied and the governing differential equations and the boundary conditions of the system are transformed into a set of algebraic equations in terms of the differential transforms of the original functions and the solution of these algebraic equations gives the desired solution of the problem. It is different from high-order Taylor series method because Taylor series method requires symbolic computation of the necessary derivatives of the data functions and is expensive for large orders. The differential transform method is an iterative procedure to obtain analytic Taylor Series solutions of differential equations. The basic definitions and the application procedure of this method can be introduced as follows:

Consider a function $f(x)$ which is analytic in a domain D and let $x=x_0$ represent any point in D. The function $f(x)$ is then represented by a power series whose center is located at $x_0$. The differential transform of the function $f(x)$ is given by

$$F[k]=\frac{1}{k!}\left(\frac{\mathrm{d}^k f(x)}{\mathrm{d}x^k}\right)_{x=x_0} \tag{38}$$

where $f(x)$ is the original function and $F[k]$ is the transformed function.

The inverse transformation is defined as

$$f(x)=\sum_{k=0}^{\infty}(x-x_0)^k F[k] \tag{39}$$

Combining Eqs. (38) and (39) gives

$$f(x)=\sum_{k=0}^{\infty}\frac{(x-x_0)^k}{k!}\left(\frac{\mathrm{d}^k f(x)}{\mathrm{d}x^k}\right)_{x=x_0} \tag{40}$$

Considering Eq. (40), once more it is noticed that the concept of differential transform is derived from Taylor series expansion. However, the method does not evaluate the derivatives symbolically.

In actual applications, the function $f(x)$ is expressed by a finite series and Eq. (40) can be written as follows:

$$f(x) = \sum_{k=0}^{m} \frac{(x - x_0)^k}{k!} \left( \frac{\mathrm{d}^k f(x)}{\mathrm{d}x^k} \right)_{x=x_0} \tag{41}$$

which means that $f(x) = \sum_{k=m+1}^{\infty} \frac{(x-x_0)^k}{k!} \left( \frac{\mathrm{d}^k f(x)}{\mathrm{d}x^k} \right)_{x=x_0}$ is negligibly small. Here, the value of $m$ depends on the convergence rate of the natural frequencies.

Theorems that are frequently used in the transformation of the differential equations and the boundary conditions are given by Tables A4 and A5, respectively, in the Appendix A.

### 4.4. Formulation with DTM

In the solution step, the differential transform method is applied to Eqs. (37a)–(37c) by using the theorems introduced in Table A4 and the following expressions are obtained:

$$c_{\mathrm{b}}c_{\mathrm{h}} \left[ \left( \frac{\mu}{\overline{\Omega}} \right)^2 - \frac{(k-2)(k+1)}{4} \right] W[k-2] + \left[ (c_{\mathrm{b}} + c_{\mathrm{h}} - \delta c_{\mathrm{b}}c_{\mathrm{h}}) \frac{(k-1)(k+1)}{3} - c_{\mathrm{b}}c_{\mathrm{h}} \left( \frac{\mu}{\overline{\Omega}} \right)^2 \right] W[k-1]$$

$$+ \left\{ \frac{k(k+1)}{2} \left[ \frac{2c_{\mathrm{b}}c_{\mathrm{h}}}{s^2\overline{\Omega}^2} + \delta(c_{\mathrm{b}} + c_{\mathrm{h}}) - 1 \right] + \left( \frac{\mu}{\overline{\Omega}} \right)^2 \right\} W[k] + (k+1)^2 \left( \delta + \frac{c_{\mathrm{b}}c_{\mathrm{h}}}{s^2\overline{\Omega}^2} \right) W[k+1]$$

$$+ \left\{ \frac{1}{2} [1 - \delta(c_{\mathrm{b}} + c_{\mathrm{h}})] + \frac{1}{3} (\delta c_{\mathrm{b}}c_{\mathrm{h}} - c_{\mathrm{b}} - c_{\mathrm{h}}) + \frac{c_{\mathrm{b}}c_{\mathrm{h}}}{4} + \frac{1}{s^2\overline{\Omega}^2} \right\} (k+1)(k+2) W[k+2]$$

$$- \frac{c_{\mathrm{b}}c_{\mathrm{h}}}{s^2\overline{\Omega}^2} (k+1)\varphi[k-1] + \frac{(c_{\mathrm{b}} + c_{\mathrm{h}})}{s^2\overline{\Omega}^2} (k+1)\varphi[k] - \frac{(k+1)}{s^2\overline{\Omega}^2} \varphi[k+1] + \bar{e} \left( \frac{\mu}{\overline{\Omega}} \right)^2 \{ c_{\mathrm{h}}c_{\mathrm{b}}^2 \psi[k-3]$$

$$+ c_{\mathrm{b}}(c_{\mathrm{b}} + 2c_{\mathrm{h}})\psi[k-2] - (2c_{\mathrm{b}} + c_{\mathrm{h}})\psi[k-1] + \psi[k] \} = 0 \tag{42a}$$

$$\frac{c_{\mathrm{b}}c_{\mathrm{h}}(k-1)}{s^2} W[k-1] - \frac{k}{s^2} (c_{\mathrm{b}} + c_{\mathrm{h}}) W[k] + \frac{(k+1)}{s^2} W[k+1] + [c_{\mathrm{b}}c_{\mathrm{h}}^3 r^2 (\overline{\Omega}^2 + \mu^2)]\varphi[k-4]$$

$$- (\overline{\Omega}^2 + \mu^2)r^2 c_{\mathrm{h}}^2 (3c_{\mathrm{b}} + c_{\mathrm{h}})\varphi[k-3] + \left[ c_{\mathrm{b}}c_{\mathrm{h}}^3 (k+1)(k-2) - \frac{c_{\mathrm{b}}c_{\mathrm{h}}}{s^2} + 3(\overline{\Omega}^2 + \mu^2)r^2 c_{\mathrm{h}}(c_{\mathrm{b}} + c_{\mathrm{h}}) \right] \varphi[k-2]$$

$$- \left[ c_{\mathrm{h}}^2 (k-1)(k+1)(3c_{\mathrm{b}} + c_{\mathrm{h}}) - \frac{c_{\mathrm{b}} + c_{\mathrm{h}}}{s^2} + (\overline{\Omega}^2 + \mu^2)r^2 (3c_{\mathrm{h}} + c_{\mathrm{b}}) \right] \varphi[k-1]$$

$$+ \left[ 3c_{\mathrm{h}}k(k+1)(c_{\mathrm{b}} + c_{\mathrm{h}}) - \frac{1}{s^2} + (\overline{\Omega}^2 + \mu^2)r^2 \right] \varphi[k] + (3c_{\mathrm{h}} + c_{\mathrm{b}})(k+1)^2 \varphi[k+1]$$

$$+ (k+1)(k+2)\varphi[k+2] + \bar{e}\overline{\Omega}^2 \{ c_{\mathrm{b}}^2 c_{\mathrm{h}} \psi[k-4] - c_{\mathrm{b}}(c_{\mathrm{b}} + 2c_{\mathrm{h}} - c_{\mathrm{b}}c_{\mathrm{h}})\psi[k-3] + [(2c_{\mathrm{b}} + c_{\mathrm{h}})$$

$$- (c_{\mathrm{b}} + 2c_{\mathrm{h}})\delta]\psi[k-2] + (2c_{\mathrm{b}}\delta + 2c_{\mathrm{h}}\delta - 1)\psi[k-1] - \delta\psi[k] \} = 0 \tag{42b}$$

$$\left(\frac{\mu}{r_\alpha \overline{\Omega}}\right)^2 \overline{e}[-c_b^2 c_h W[k-3] + c_b(c_b + 2c_h)W[k-2] - (2c_b + c_h)W[k-1] + W[k]]$$

$$+ \frac{\overline{e}}{r_\alpha^2}[c_b^2 c_h \varphi[k-4] - c_b(c_b + 2c_h - c_b c_h \delta)\varphi[k-3] + (2c_b + c_h - c_b^2 \delta - 2c_b c_h \delta)\varphi[k-2]$$

$$+ (2c_b \delta + c_h \delta - 1)\varphi[k-1] - \delta\varphi[k]] - c_b c_h^3 \left[\left(\frac{r^2}{r_\alpha^2} + \frac{\mu^2}{\overline{\Omega}^2}\right) - \frac{(k-4)(k+1)}{4}\right]\psi[k-4]$$

$$+ c_h^2 \left[(k-3)(k+1)\left(\frac{5}{6}c_b + \frac{1}{3}c_h - c_b c_h \delta\right) - \left(\frac{r^2}{r_\alpha^2} + \frac{\mu^2}{\overline{\Omega}^2}\right)(3c_b + c_h)\right]\psi[k-3]$$

$$+ \left\{(k-2)(k+1)\left[-\frac{11}{12}c_b c_h - \frac{7}{6}c_h^2 + \delta\left(\frac{7}{6}c_b c_h^2 + \frac{1}{2}c_h^3\right) + \left(\frac{\sigma}{r_\alpha \overline{\Omega}}\right)^2 c_b c_h^3\right]\right.$$

$$\left. + 3\left(\frac{r^2}{r_\alpha^2} + \frac{\mu^2}{\overline{\Omega}^2}\right)c_h(c_b + c_h)\right\}\psi[k-2]$$

$$+ \left[\frac{1}{3}(k-1)(k+1)(c_b + 4c_h) - \left(\frac{r^2}{r_\alpha^2} + \frac{\mu^2}{\overline{\Omega}^2}\right)(c_b + 3c_h) - \left(\frac{\sigma}{r_\alpha \overline{\Omega}}\right)^2 (k-1)(k+1)c_h^2(3c_b + c_h)\right.$$

$$\left. - \frac{2}{3}c_h(2c_b + 3c_h)(k-1)(k+1)\delta\right]\psi[k-1] + \frac{1}{2}k(k+1)\left[\left(c_h^2 - \frac{2}{3}c_b c_h^2 - \frac{2}{3}c_h^3 + \frac{1}{2}c_b c_h^3 - 1\right)\right.$$

$$\left. + \left(\frac{r^2}{r_\alpha^2} + \frac{\mu^2}{\overline{\Omega}^2}\right) + \delta\left(c_b + 5c_h + 2c_h^2 - c_b c_h^2 - c_h^3 + \frac{1}{3}c_b c_h^3\right) + 6\left(\frac{\sigma}{r_\alpha \overline{\Omega}}\right)^2 (c_b c_h + c_h^2)\right]\psi[k]$$

$$+ (k+1)^2 \left[c_h\left(\frac{2}{3}c_b + \frac{2}{3}c_h - \frac{1}{2}c_b c_h - 1\right) + \delta\left(c_b c_h + c_h^2 - \frac{2}{3}c_b c_h^2 - 2c_h - 1\right)\right.$$

$$\left. - \left(\frac{\sigma}{r_\alpha \overline{\Omega}}\right)^2 (c_b + 3c_h)\right]\psi[k+1] + \left\{\frac{1}{2} - \frac{1}{3}(c_b + c_h) + \frac{1}{4}c_b c_h + \delta\left[1 - \frac{1}{2}(c_b + c_h)\right.\right.$$

$$\left.\left. + \frac{1}{3}c_b c_h\right] + \left(\frac{\sigma}{r_\alpha \overline{\Omega}}\right)^2\right\}\psi[k+2] \tag{42c}$$

Here, $\varphi[k]$, $W[k]$ and $\psi[k]$ are the transformed functions of $\overline{\varphi}$, $\tilde{w}$, $\overline{\psi}$, respectively.

Furthermore, applying the differential transform method to Eqs. (29a) and (30a)–(30c), the transformed boundary conditions are obtained as follows:

$$\text{at } \overline{x} = 0 \Rightarrow \varphi[0] = W[0] = \psi[0] = 0 \tag{43a}$$

$$\text{at } \overline{x} = 1 \Rightarrow (k+1)\varphi[k+1] + \overline{e}\frac{\mu^2}{\overline{\Omega}^2}(k+1)\psi[k+1] = 0 \tag{43b}$$

$$\left[\overline{\Omega}^2 r^2 \left(1 + \frac{\mu^2}{\overline{\Omega}^2}\right) - \frac{1}{s^2}\right](k+1)W[k+1] - \varphi[k] = 0 \tag{43c}$$

$$\left(\frac{\sigma^2}{\overline{\Omega}^2 r_\alpha^2}\right)(k+1)\psi[k+1] - \left(\frac{\delta}{r_\alpha^2}\overline{e}\right)(k+1)\varphi[k+1] = 0 \tag{43d}$$

Substituting the boundary conditions expressed in Eqs. (43a)–(43d) into Eqs. (42a)–(42c) and taking $\varphi[1] = c_1$, $W[1] = c_2$, $\psi[1] = c_3$, the following expression is obtained

$$A_{j1}^{(n)}(\omega)c_1 + A_{j2}^{(n)}(\omega)c_2 + A_{j3}^{(n)}(\omega)c_3 = 0, \quad j = 1, 2, 3 \tag{44}$$

where $c_1$, $c_2$ and $c_3$ are constants and $A_{j1}^{(n)}(\omega), A_{j2}^{(n)}(\omega), A_{j3}^{(n)}(\omega)$ are polynomials of $\omega$ corresponding to $n$.

The matrix form of Eq. (44) can be given by

$$\begin{bmatrix} A_{11}^{(n)}(\omega) & A_{12}^{(n)}(\omega) & A_{13}^{(n)}(\omega) \\ A_{21}^{(n)}(\omega) & A_{22}^{(n)}(\omega) & A_{23}^{(n)}(\omega) \\ A_{31}^{(n)}(\omega) & A_{32}^{(n)}(\omega) & A_{33}^{(n)}(\omega) \end{bmatrix} \begin{Bmatrix} c_1 \\ c_2 \\ c_3 \end{Bmatrix} = \begin{Bmatrix} 0 \\ 0 \\ 0 \end{Bmatrix} \tag{45}$$

The eigenvalues are calculated by taking the determinant of the $[A_{ji}]$ matrix.

$$\begin{vmatrix} A_{11}^{(n)}(\omega) & A_{12}^{(n)}(\omega) & A_{13}^{(n)}(\omega) \\ A_{21}^{(n)}(\omega) & A_{22}^{(n)}(\omega) & A_{23}^{(n)}(\omega) \\ A_{31}^{(n)}(\omega) & A_{32}^{(n)}(\omega) & A_{33}^{(n)}(\omega) \end{vmatrix} = 0 \tag{46}$$

Solving Eq. (46), the eigenvalues are calculated. The $j$th estimated eigenvalue, $\omega_j^{(n)}$ corresponds to $n$ and the value of $n$ is determined by the following equation:

$$\left| \omega_j^{(n)} - \omega_j^{(n-1)} \right| \leqslant \varepsilon \tag{47}$$

where $\omega_j^{(n-1)}$ is the $j$th estimated eigenvalue corresponding to $n-1$ and where $\varepsilon$ is the tolerance parameter. If Eq. (47) is satisfied, then the $j$th eigenvalue, $\omega_j^{(n)}$, is obtained. In general, $\omega_j^{(n)}$ are conjugated complex values, and can be written as $\omega_j^{(n)} = a_j + ib_j$. Neglecting the small imaginary part $b_j$, the $j$th natural frequency, $a_j$, is found.

## 5. Results and discussions

At first glance, application of the differential transform method to both the equations of motion and the boundary conditions seem to be very involved computationally. However, all the algebraic calculations are finished quickly by using a symbolic computational software. The computer package Mathematica is used to write a code for the expressions given by Eqs. (42a)–(42c), (43b)–(43d). The natural frequencies are calculated, the mode shapes are plotted and the effects of the rotational speed, hub radius, slenderness ratio, bending–torsion coupling and taper ratios are investigated. Additionally, a rotating Timoshenko beam model that tapers linearly in both planes with respect to the same taper ratio ($c_b = c_h$) is created and analysed in the finite element program, ABAQUS and some illustrative examples which study simpler beam models are found in open literature and solved in order to make comparisons. Consequently, it is observed that there is a good agreement between the results.

In Fig. 4, convergence of the first six natural frequencies are introduced. Here, it was necessary to take 50 terms to evaluate up to the sixth natural frequency to five-digit precision. Therefore, the number of the terms, $m$, mentioned in Eq. (41) is 50 for the first six natural frequencies. Additionally, here it is seen that higher modes appear when more terms are taken into account in DTM application. Thus, depending on the order of the required mode, one must try a few values for the term number at the beginning of the Mathematica calculations in order to find the adequate number of terms.

In Fig. 5(a)–(e), the first five normal mode shapes of a rotating Timoshenko beam featuring bending–torsion coupling are introduced. Here, it is observed that the first, the second and the fourth normal modes are dominated by bending while in the third and the fifth normal modes, torsion is dominant.

In Table 1, variation of the first six natural frequencies, $\omega$, with respect to the rotational speed, $\Omega$, is introduced for the beam properties given below. Additionally, the results taken from ABAQUS are included for validation and it is observed that there is a good agreement between the results of this study and the ABAQUS results:

$$GJ_0 = 1.12599 \times 10^6 \text{ N m}^2 \quad I_{y0} = 1.17187 \times 10^{-5} \text{ m}^4 \quad I_{\alpha0} = 0.5015 \text{ kg m}$$
$$E = 70 \times 10^9 \text{ N/m}^2 \quad kA_0G = 5.93654 \times 10^8 \text{ N} \quad \rho A = 72 \text{ kg/m}$$
$$L = 1 \text{ m} \quad c_b = c_h = 0.5 \quad e_0 = 9.30 \times 10^{-3} \text{ m}$$
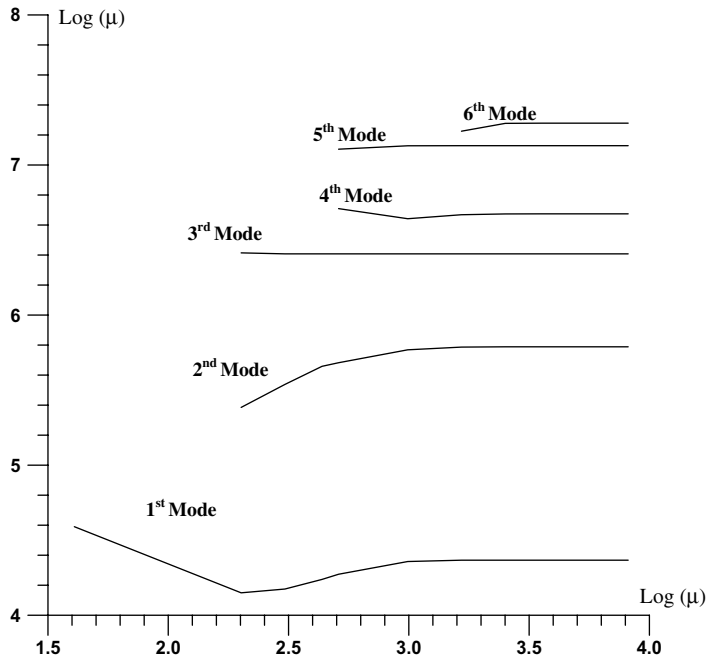
Fig. 4. Convergence of the first six natural frequencies.

For further validation, in Table 2 the results are compared with the ones calculated by Eslimy-Isfahany and Banerjee [36] for the values given below. In this example, a nonrotating, uniform Timoshenko beam featuring bending–torsion coupling is considered.

$$GJ_0 = 9.88 \times 10^5 \text{ N m}^2 \quad EI_{y0} = 9.75 \times 10^6 \text{ N m}^2 \quad I_{z0} = 8.65 \text{ kg m}$$
$$\rho A_0 = 35.75 \text{ kg/m} \quad kA_0 G = 296\,154\,000 \text{ N} \quad e_0 = -0.18 \text{ m}$$
$$L = 6 \text{ m} \quad c_b = c_h = 0$$

In order to investigate the effect of the rotational speed more deeply, the tapered beam natural frequencies are given in tabular form in Table 3 where the taper ratios are chosen to be $c_b = c_h = 0.4$. Here, it is observed that the natural frequencies increase with the increasing rotational speed parameter, $\overline{\Omega}$. The increase in the frequency due to rotation is 63% for the first bending mode, 16% for the second bending mode, 6% for the third bending mode and 3.5% for the fourth bending mode. Comparing the percentage increase in the bending frequencies, it is noticed that the effect of the rotational speed is dominant on the fundamental bending mode and this effect diminishes rapidly as the frequency order increases. Moreover, the increase of frequency due to rotation is 1.8% for the first torsion mode while it is 1.6% for the second torsion mode. Therefore, the effect of rotation on the torsion modes is insignificant even when it is compared with the low bending frequencies.

Effects of the breadth taper ratio, $c_b$, and the height taper ratio, $c_h$, on the natural frequencies are introduced in Fig. 6 and 7, respectively. Examining these figures, the following results are obtained:

- The breadth taper ratio has an increasing effect on both the bending and torsion natural frequencies.
- The height taper ratio has an increasing effect on the first bending mode. The other bending frequencies decrease as the height taper ratio increases up to a certain value called the critical taper ratio after which the natural frequencies reverse their trend of change as reported by Bazoune and Khulief [37] and Khulief and Bazoune [38].
- The torsional frequencies initially increase with the increasing height taper ratio and then decrease after some critical taper ratio.

In Table 4, variation of the natural frequencies with respect to different combinations of the taper ratios is introduced. The results, which are calculated for $r = 0.08$, $\overline{\Omega} = 0$ and the Poisson ratio, $v = 0.3$, are compared
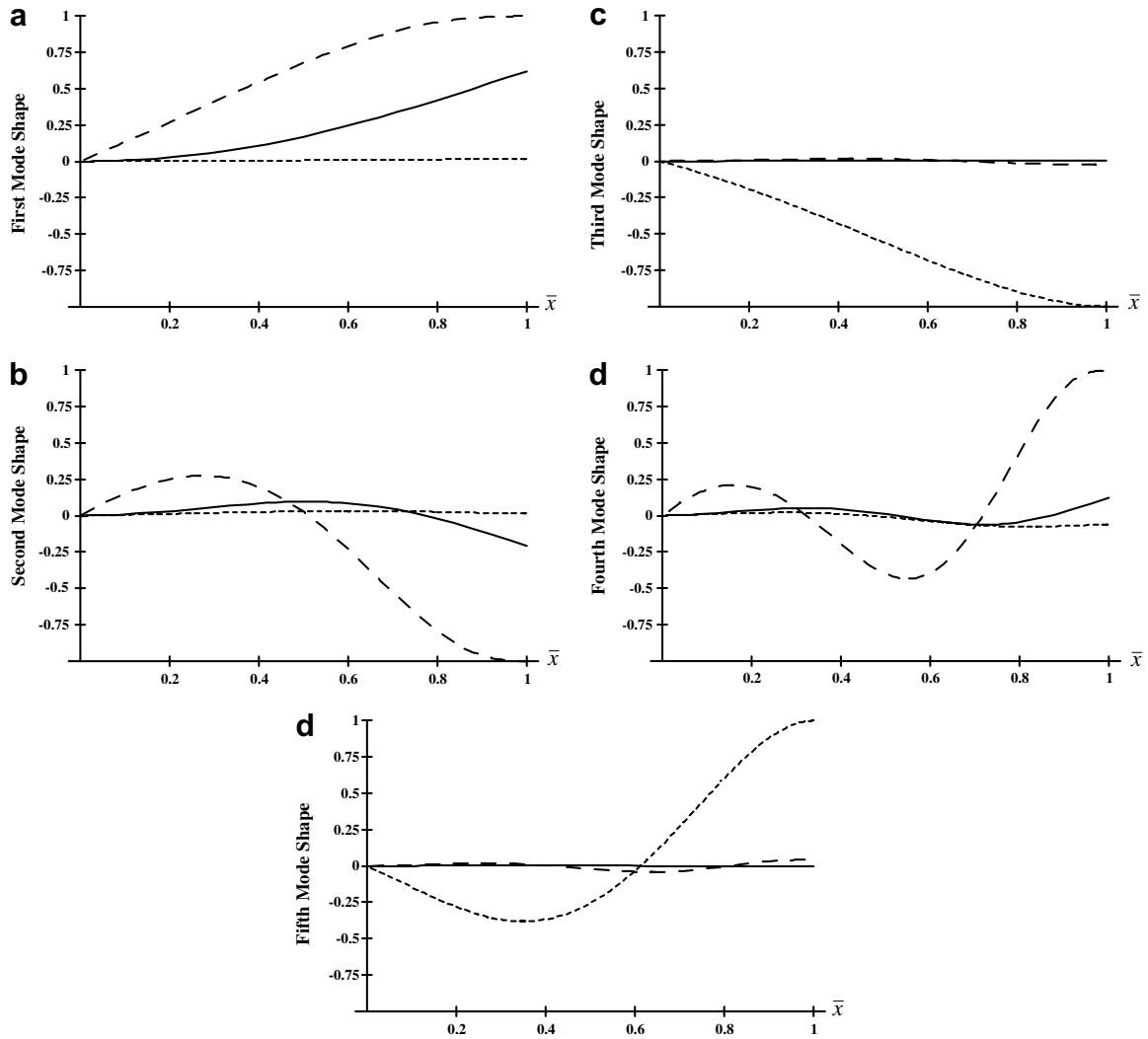
Fig. 5. The normal mode shapes of the rotating coupled Timoshenko beam (—: $w$; –––: $\varphi$, - - -,: $\psi$).

Table 1
Variation of the natural frequencies with respect to the rotational speed, $\Omega$

| Rotational speed (rad/s) | | | | | | | |
|---|---|---|---|---|---|---|---|
| 5 | | 20 | | 50 | | 100 | |
| Present | ABAQUS | Present | ABAQUS | Present | ABAQUS | Present | ABAQUS |
| Natural frequencies (Hz) | | | | | | | |
| 78.2499 | 78.267 | 78.3286 | 78.341 | 78.7682 | 78.750 | 80.3164 | 80.192 |
| 325.946 | 326.06 | 326.02 | 326.13 | 326.436 | 326.52 | 327.916 | 327.90 |
| 606.437 | 606.40 | 606.45 | 606.42 | 606.518 | 606.54 | 606.764 | 606.98 |
| 791.408 | 791.89 | 791.48 | 791.95 | 791.883 | 792.30 | 793.32 | 793.54 |
| 1247.08 | 1246.8 | 1247.11 | 1246.9 | 1247.23 | 1247.1 | 1247.69 | 1247.9 |
| 1449.38 | 1450.7 | 1449.46 | 1450.7 | 1449.86 | 1451.1 | 1451.3 | 1452.1 |

with the ones calculated by Downs [39]. The torsion frequencies that are not included by Downs [39] are also added. Here, a very good agreement between the results is observed. In this example, a nonrotating, double tapered and uncoupled Timoshenko beam model is studied.

Table 2
Natural frequencies of nonrotating, uniform Timoshenko beam featuring bending–torsion coupling

| Natural frequencies | |
|---|---|
| Present | Ref. [36] |
| 49.4803 | 49.6 |
| 97.0028 | 97.0 |
| 247.631 | 248.9 |
| 350.921 | 355.6 |
| 449.395 | 451.5 |
| 609.273 | 610.1 |
| 790.255 | – |
| 929.155 | – |

Table 3
Effect of the rotational speed parameter on the natural frequencies

| $\overline{\Omega}$ | | | | |
|---|---|---|---|---|
| 1 | 2 | 3 | 4 | 5 |
| Bending frequencies | | | | |
| 73.06 | 75.52 | 82.42 | 92.69 | 105.26 |
| 333.55 | 335.84 | 342.64 | 353.68 | 368.56 |
| 831.55 | 833.78 | 840.46 | 851.46 | 866.60 |
| 1531.19 | 1533.46 | 1540.23 | 1551.45 | 1567.00 |
| Torsion frequencies | | | | |
| 544.57 | 544.95 | 546.09 | 547.98 | 550.63 |
| 1208.63 | 1209.38 | 1211.65 | 1215.41 | 1220.66 |

In Table 5, effects of the bending–torsion coupling, the rotary inertia and the shear deformation are investigated and the results are tabulated for the rotational speed, $\Omega = 50$ rad/s. Examining Table 5, the following results are obtained:

- As noted by Subrahmanyam et al. [3], bending–torsion coupling has a decreasing effect on the bending based natural frequencies (the first, the second, the fourth and the sixth ones) while it has an increasing effect on the torsion based frequencies (the third and the fifth ones).
- Rotary inertia and shear deformation effects that are results of the Timoshenko Beam Theory have a decreasing effect on the bending based natural frequencies. Therefore, the bending based natural frequencies of the coupled Timoshenko beam are lower than the natural frequencies of the coupled Euler–Bernoulli beam. However, rotary inertia and shear deformation have almost no effect on the torsion based natural frequencies.
- Both the coupling effect and the Timoshenko effects are more significant on the higher modes.

In Table 6, the effect of the hub radius parameter, $\delta$, is investigated for several rotational speed values. As introduced in Table 3, natural frequencies increase with the increasing rotational speed. In Table 6, it is noticed that this rate of increase becomes larger with the increasing hub radius parameter, $\delta$ because the centrifugal force, Eq. (14), is directly proportional to the hub radius, $R$. For a better insight and also in order to establish the trend, these effects are shown in Fig. 8 where the fundamental natural frequency is plotted for three different values of the hub radius parameter, $\delta$, and for several rotational speed values, $\Omega$.

In Table 7, effect of the $\rho I_y \Omega^2 \varphi$ term is observed. Comparisons are made with Banerjee [35] where the term is included and Lee and Kuo [34] where it is neglected. As it is seen in the error section of Table 7, percentage error increases with the increasing rotational speed parameter. Here, the results are given for $c_h = c_b = 0$, $\delta = 0$, $r = 1/30$ and $E/kG = 3.059$ values.
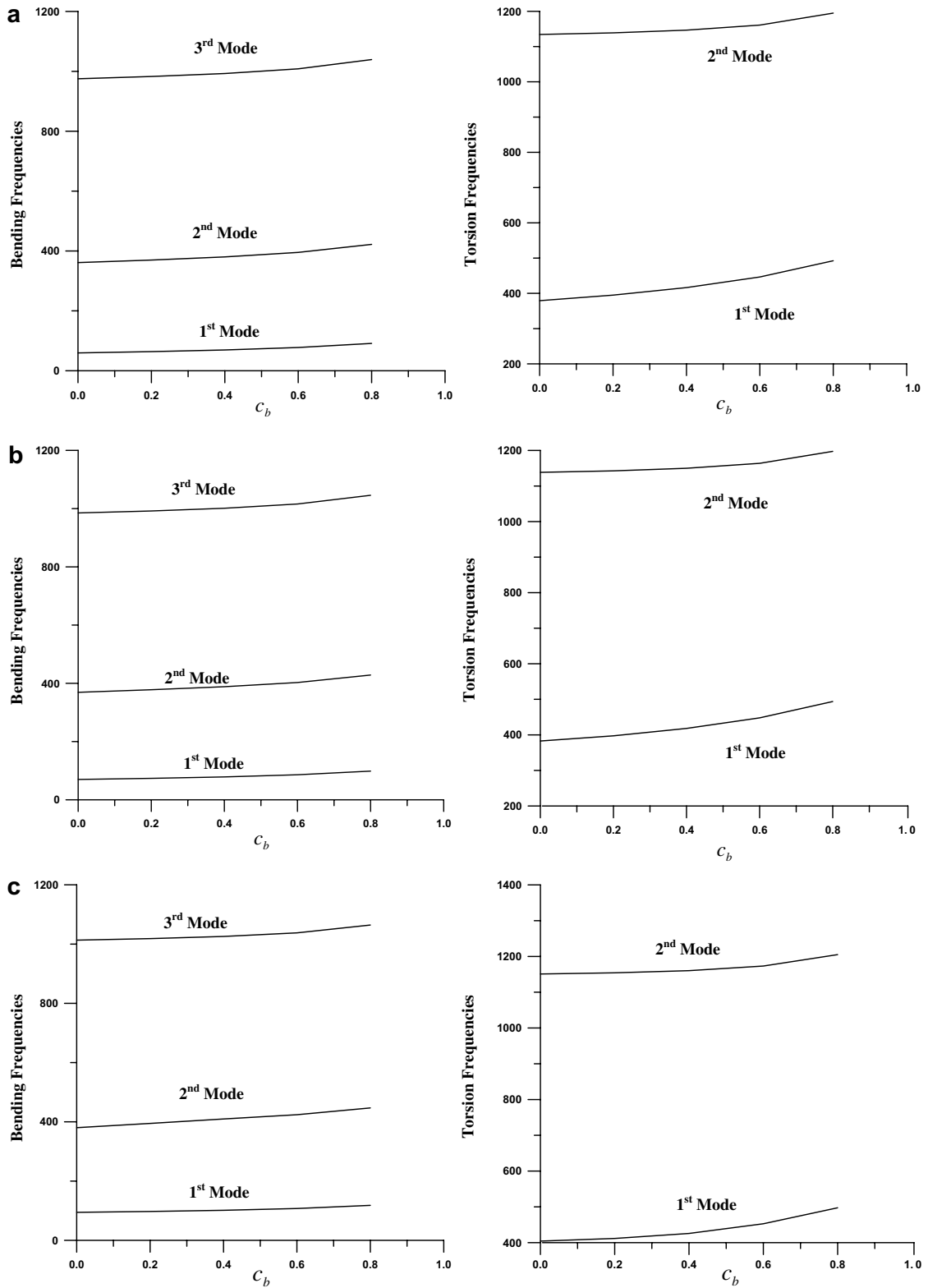
Fig. 6. Effect of the breadth taper ratio for (a) $\overline{\Omega} = 0$, (b) $\overline{\Omega} = 2$ and (c) $\overline{\Omega} = 4$.
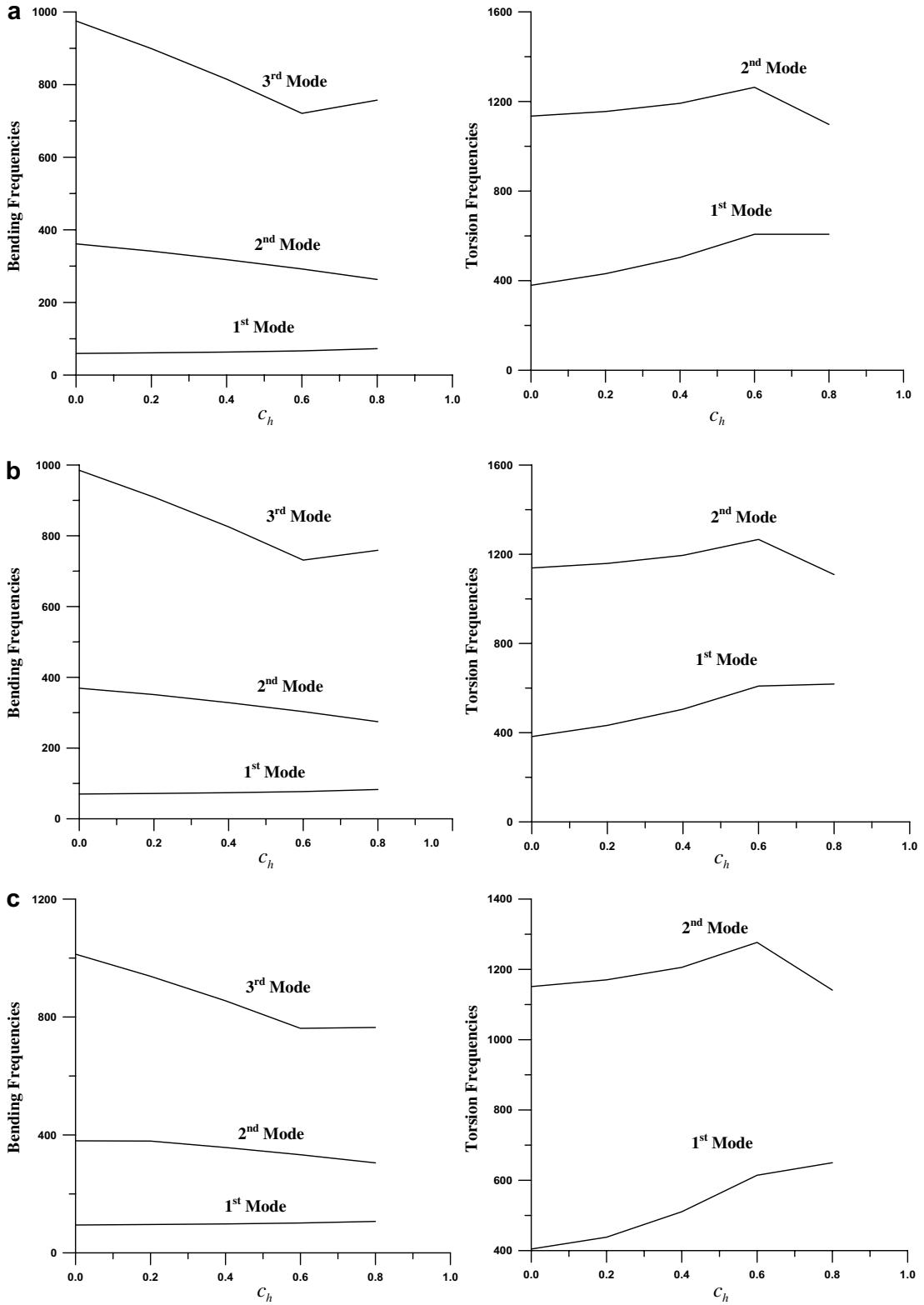
Fig. 7. Effect of the height taper ratio for (a) $\overline{\Omega} = 0$, (b) $\overline{\Omega} = 2$ and (c) $\overline{\Omega} = 4$.

Table 4
Variation of the natural frequencies of a nonrotating Timoshenko beam with different combinations of breadth and height taper ratios

| Frequency type | $c_h$ | | | | | | | | |
|---|---|---|---|---|---|---|---|---|---|
| | 0 | | | 0.3 | | | 0.6 | | |
| | $c_b$ | | | $c_b$ | | | $c_b$ | | |
| | 0 | 0.3 | 0.6 | 0 | 0.3 | 0.6 | 0 | 0.3 | 0.6 |
| Bending frequencies | 3.32404 | 3.68722 | 4.28828 | 3.48689 | 3.85345 | 4.46106 | 3.76227 | 4.13388 | 4.74978 |
| | 3.32400[a] | 3.68723[a] | 4.28829[a] | 3.48689[a] | 3.85346[a] | 4.46107[a] | 3.76228[a] | 4.13389[a] | 4.74979[a] |
| | 16.2889 | 16.8750 | 17.7869 | 15.6409 | 16.1764 | 17.0227 | 14.6448 | 15.1296 | 15.9106 |
| | 16.2890[a] | 16.8752[a] | 17.7871[a] | 15.6411[a] | 16.1766[a] | 17.0229[a] | 14.6449[a] | 15.1297[a] | 15.9107[a] |
| | 36.7073 | 37.1583 | 37.9216 | 34.6621 | 35.1022 | 35.8342 | 31.6239 | 32.0578 | 32.7688 |
| | 36.7078[a] | 37.1588[a] | 37.9221[a] | 34.6625[a] | 35.1026[a] | 35.8346[a] | 31.6243[a] | 32.0582[a] | 32.7693[a] |
| | 58.2778 | 58.6862 | 59.4326 | 55.9271 | 56.3072 | 56.9717 | 51.6225 | 51.9987 | 52.6309 |
| | 58.2788[a] | 58.6872[a] | 59.4336[a] | 55.9280[a] | 56.3081[a] | 56.9726[a] | 51.6225[a] | 51.9995[a] | 52.6316[a] |
| Torsion frequencies | 22.0510 | 23.6630 | 26.1670 | 27.0340 | 28.7860 | 31.4680 | 35.0790 | 36.9730 | 39.7710 |
| | – | – | – | – | – | – | – | – | – |
| | 66.1530 | 66.7360 | 67.9420 | 68.1480 | 68.9700 | 70.5230 | 72.9950 | 73.7300 | 74.2840 |
| | – | – | – | – | – | – | – | | |

[a] Downs [39].

Table 5
Effects of the bending–torsion coupling, rotary inertia and shear deformation on the natural frequencies

| Frequency order | Natural frequencies (Hz) | | |
|---|---|---|---|
| | Coupled Timoshenko | Uncoupled Timoshenko | Coupled Euler |
| 1 | 78.7682 | 78.7752 | 79.0893 |
| 2 | 326.436 | 326.666 | 332.302 |
| 3 | 606.518 | 602.579 | 606.547 |
| 4 | 791.883 | 793.103 | 822.987 |
| 5 | 1247.23 | 1238.53 | 1247.57 |
| 6 | 1449.86 | 1454.32 | 1522.75 |

Table 6
Effects of the hub radius and the rotational speed on the natural frequencies

| $\delta$ | $\Omega$ | | | | | |
|---|---|---|---|---|---|---|
| | 0 | 10 | 20 | 30 | 40 | 50 |
| | *Natural frequencies (Hz)* | | | | | |
| 0 | 78.2446 | 78.2656 | 78.3286 | 78.4335 | 78.5801 | 78.7682 |
| | 325.941 | 325.961 | 326.020 | 326.119 | 326.258 | 326.436 |
| | 606.437 | 606.440 | 606.450 | 606.466 | 606.489 | 606.518 |
| 0.2 | 78.2446 | 78.2713 | 78.3513 | 78.4845 | 78.6706 | 78.9091 |
| | 325.941 | 325.966 | 326.042 | 326.167 | 326.343 | 326.569 |
| | 606.437 | 606.441 | 606.454 | 606.477 | 606.508 | 606.548 |
| 0.4 | 78.2446 | 78.277 | 78.374 | 78.5355 | 78.761 | 79.0498 |
| | 325.941 | 325.972 | 326.063 | 326.215 | 326.428 | 326.702 |
| | 606.437 | 606.442 | 606.459 | 606.487 | 606.527 | 606.577 |
| 0.6 | 78.2446 | 78.2827 | 78.3967 | 78.5864 | 78.8512 | 79.1903 |
| | 325.941 | 325.977 | 326.084 | 326.263 | 326.513 | 326.835 |
| | 606.437 | 606.443 | 606.464 | 606.498 | 606.546 | 606.607 |
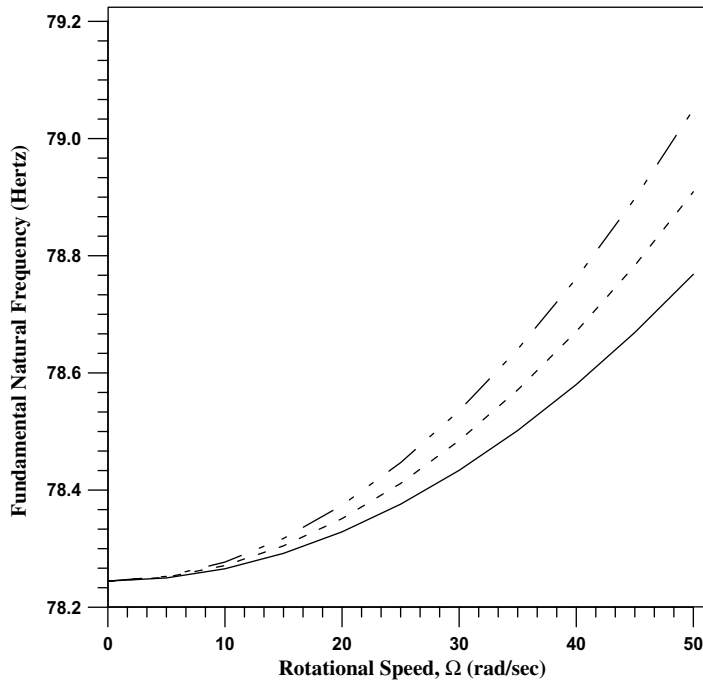
Fig. 8. Effects the hub radius parameter, $\delta$ and the rotational speed, $\Omega$ on the fundamental natural frequency ($\delta = 0.4$, –·–·–; $\delta = 0.2$, ---; $\delta = 0$, —).

Table 7
Effect of the $\rho I_y \Omega^2 \varphi$ term on the natural frequencies

Natural frequency parameter ($\mu$)

| $\overline{\Omega}$ | Modes | Present | Ref. [35] | Ref. [34] | Error (%) |
|---|---|---|---|---|---|
| 0 | Bending | 3.47984 | 3.4798 | 3.4798 | 0.00115 |
| | | 20.5891 | – | – | – |
| | | 53.3396 | – | – | – |
| | Torsion | 22.051 | – | – | – |
| | | 66.153 | – | – | – |
| 1 | Bending | 3.64452 | 3.6445 | 3.6452 | 0.01866 |
| | | 20.7375 | – | – | – |
| | | 53.4941 | – | – | – |
| | Torsion | 22.0717 | – | – | – |
| | | 66.2096 | – | – | – |
| 2 | Bending | 4.0971 | 4.0971 | 4.0994 | 0.05589 |
| | | 21.1766 | – | – | – |
| | | 53.9544 | – | – | – |
| | Torsion | 222.1336 | | | – |
| | | 66.379 | | | – |
| 3 | Bending | 4.75157 | 4.7516 | 4.7558 | 0.08902 |
| | | 21.8883 | – | – | – |
| | | 54.7112 | – | – | – |
| | Torsion | 22.2364 | – | – | – |
| | | 66.6598 | – | – | – |
| 4 | Bending | 5.5314 | 5.5314 | 5.5375 | 0.11028 |
| | | 22.8466 | – | – | – |
| | | 55.7505 | – | – | – |
| | Torsion | 22.3793 | – | – | – |
| | | 67.0500 | – | – | – |

## 6. Conclusion

Using the Hamilton's principle, the governing differential equations of motion for a cantilevered, rotating, double tapered Timoshenko beam, featuring coupling between flapwise bending and torsion vibrations, are derived and solved by applying the differential transform method (DTM). The main contributions of this study to the literature appear in the derivation of the governing differential equations and they can be listed as follows:

- In the study of Hodges and Dowell [32], the Euler–Bernoulli Beam Theory is used and in the present study, their formulation is modified for the Timoshenko Beam Theory and a new expression, $\gamma = w' - \varphi = O(\varepsilon^2)$, is added to their ordering scheme as a contribution to the literature.
- In this study, the missing term, $\rho I_y \Omega^2 \varphi$, appears in the governing differential equations of motion as a result of the Hamilton's principle application to the derived energy expressions,. Examining the derivations, it can be easily understood where it comes from.
- Any study that considers rotating, double tapered, bending–torsion coupled Timoshenko beam is not present in open literature. Therefore, in order to validate the calculated results, the beam model studied in this paper is created and analysed using a finite element program, ABAQUS.

Additionally, the effects of several parameters are examined in this study and the following results are obtained:

- Increasing rotational speed parameter, $\overline{\Omega}$, hub radius parameter, $\delta$ and breadth taper ratio parameter, $c_b$ have an increasing effect on all the natural frequencies.
- The height taper ratio, $c_h$, has an increasing effect on the torsional frequencies and the first bending frequency while it has a decreasing effect on the rest of the bending frequencies.
- Bending–torsion coupling has a decreasing effect on the bending frequencies while it has an increasing effect on the torsional frequencies.
- Rotary inertia and shear deformation effects have a decreasing effect on the bending frequencies while they have almost no effect on the torsional frequencies.

## Appendix A

See Tables A1–A5.

Table A1
Ordering scheme for bending–torsion coupled Timoshenko beam formulation

| | |
|---|---|
| $\frac{x}{R} = O(1)$ | $\frac{\xi}{R} = O(\varepsilon)$ |
| $\frac{w}{R} = O(\varepsilon)$ | $\frac{\eta}{R} = O(\varepsilon)$ |
| $\varphi = O(\varepsilon)$ | $\psi = O(\varepsilon)$ |
| $\frac{u_0}{R} = O(\varepsilon^2)$ | $\gamma = w' - \varphi = O(\varepsilon^2)$ |

Table A2
Area integrals for potential energy expression

| | | |
|---|---|---|
| $\int\int_A \mathrm{d}\eta\,\mathrm{d}\xi = A$ | $\int\int_A \eta^2\mathrm{d}\eta\,\mathrm{d}\xi = I_z$ | $\int\int_A \xi^2\mathrm{d}\eta\,\mathrm{d}\xi = I_y$ |
| $\int\int_A \eta\,\mathrm{d}\eta\,\mathrm{d}\xi = Ae$ | $\int\int_A (\eta^2 + \xi^2)\mathrm{d}\eta\,\mathrm{d}\xi = J$ | $\int\int_A \xi\mathrm{d}\eta\,\mathrm{d}\xi = \int\int_A \eta\xi\mathrm{d}\eta\,\mathrm{d}\xi = 0$ |

Table A3
Area integrals for kinetic energy expression

| | | |
|---|---|---|
| $\int\int_A \rho \, \mathrm{d}\eta \, \mathrm{d}\xi = \rho A$ | $\int\int_A \rho\eta^2 \mathrm{d}\eta \, \mathrm{d}\xi = \rho I_z$ | $\int\int_A \rho\xi^2 \mathrm{d}\eta \, \mathrm{d}\xi = \rho I_y$ |
| $\int\int_A \rho\eta \, \mathrm{d}\eta \, \mathrm{d}\xi = \rho Ae$ | $\int\int_A \rho(\eta^2 + \xi^2) \mathrm{d}\eta \, \mathrm{d}\xi = I_\alpha$ | $\int\int_A \rho\xi \, \mathrm{d}\eta \, \mathrm{d}\xi = \int\int_A \rho\eta\xi \, \mathrm{d}\eta \, \mathrm{d}\xi = 0$ |

Table A4
DTM theorems used for equations of motion

| Original function | Transformed function |
|---|---|
| $f(x) = g(x) \pm h(x)$ | $F[k] = G[k] \pm H[k]$ |
| $f(x) = \lambda g(x)$ | $F[k] = \lambda G[k]$ |
| $f(x) = g(x)h(x)$ | $F[k] = \sum_{l=0}^{k} G[k-l]H[l]$ |
| $f(x) = \frac{\mathrm{d}^n g(x)}{\mathrm{d}x^n}$ | $F[k] = \frac{(k+n)!}{k!} G[k+n]$ |
| $f(x) = x^n$ | $F[k] = \delta(k-n) = \begin{cases} 0 & \text{if } k \neq n \\ 1 & \text{if } k = n \end{cases}$ |

Table A5
DTM theorems used for boundary conditions

| $x = 0$ | | $x = 1$ | |
|---|---|---|---|
| Original B.C. | Transformed B.C. | Original B.C. | Transformed B.C. |
| $f(0) = 0$ | $F(0) = 0$ | $f(1) = 0$ | $\sum_{k=0}^{\infty} F(k) = 0$ |
| $\frac{\mathrm{d}f}{\mathrm{d}x}(0) = 0$ | $F(1) = 0$ | $\frac{\mathrm{d}f}{\mathrm{d}x}(1) = 0$ | $\sum_{k=0}^{\infty} kF(k) = 0$ |
| $\frac{\mathrm{d}^2 f}{\mathrm{d}x^2}(0) = 0$ | $F(2) = 0$ | $\frac{\mathrm{d}^2 f}{\mathrm{d}x^2}(1) = 0$ | $\sum_{k=0}^{\infty} k(k-1)F(k) = 0$ |
| $\frac{\mathrm{d}^3 f}{\mathrm{d}x^3}(0) = 0$ | $F(3) = 0$ | $\frac{\mathrm{d}^3 f}{\mathrm{d}x^3}(1) = 0$ | $\sum_{k=0}^{\infty} (k-1)(k-2)kF(k) = 0$ |

# References

[1] J.C. Houbolt, C.W. Brooks, National Advisory Committee for Aeronautics Report 1346, 1958.
[2] R.E.D. Bishop, W.G. Price, J. Sound Vib. 50 (1977) 469–477.
[3] K.B. Subrahmanyam, S.V. Kulkarni, J.S. Rao, J. Sound Vib. 75 (1) (1981) 17–36.
[4] W.L. Hallauer, R.Y.L. Liu, J. Sound Vib. 85 (1982) 105–113.
[5] P.O. Friberg, Int. J. Numer. Meth. Eng. 19 (1983) 479–493.
[6] E. Dokumacı, J. Sound Vib. 119 (1987) 443–449.
[7] R.E.D. Bishop, S.M. Cannon, S. Miao, J. Sound Vib. 131 (1989) 457–464.
[8] V. Karadag, J. Sound Vib. 8 (1984) 183–197.
[9] V. Karadag, J. Sound Vib. 92 (4) (1984) 471–490.
[10] J.R. Banerjee, F.W. Williams, Comput Struct. 42 (1992) 301–310.
[11] J.R. Banerjee, F.W. Williams, Int. J. Solids Struct. 31 (1994) 749–762.
[12] J.R. Banerjee, S. Guo, W.P. Howson, Comput Struct 59 (1996) 612–621.
[13] S.H.R. Eslimy-Isfahany, J.R. Banerjee, A.J. Sobey, J. Sound Vib. 195 (2) (1996) 267–283.
[14] A.N. Bercin, M. Tanaka, J. Sound Vib. 207 (1) (1997) 47–59.
[15] S.M. Hashemi, M.J. Richard, Comput. Struct. 77 (2000) 711–724.
[16] M. Sabuncu, K. Evran, Int. J. Mech. Sci. 48 (2006) 579–590.
[17] M. Sabuncu, K. Evran, Finite Elem. Anal. Des. 41 (2005) 1011–1026.
[18] M.O. Kaya, Aircr. Eng. Aerosp. Tech. 78 (3) (2006) 194–203.
[19] O. Ozdemir Ozgumus, M.O. Kaya, MECCANICA 2006 41 (6) (2006) 661–670.
[20] Ö. Özdemir, M.O. Kaya, J. Sound Vib. 289 (2006) 413–420.
[21] Ö. Özdemir, M.O. Kaya, Flexural–torsional coupled vibration analysis of a thin-walled closed section composite Timoshenko beam by using the differential transform method, in: The Seventh International Conference on Vibration Problems (ICOVP-2005), Turkey, 2005, pp. 279–284.
[22] Ö. Özdemir, M.O. Kaya, Free vibration analysis of a rotating tapered Timoshenko beam, in: Third Ankara International Aerospace Conference, Turkey, 2005 (on CD).
[23] J.K. Zhou, Differential Transformation and Its Application for Electrical Circuits, Huazhong University Press, PR China, 1986 (in Chinese).
[24] J.S. Chiou, J.R. Tzeng, J. Vib. Acoust. 118 (1996) 83–87.
[25] M.J. Jang, C.L. Chen, Y.C. Liu, Appl. Math. Comput. 121 (2001) 261–270.

[26] I.H. Abdel, H. Hassan, Appl. Math. Comput. 127 (2002) 1–22.
[27] A. Arikoglu, I. Ozkol, Appl. Math. Comput. 168 (2005) 1145–1158.
[28] A. Arikoglu, I. Ozkol, Appl. Math. Comput. 181 (2006) 153–162.
[29] O. Ozdemir Ozgumus, M.O. Kaya, Aircr. Eng. Aerosp. Tech. 79 (2) (2007) 177–183.
[30] O. Ozdemir Ozgumus, M.O. Kaya, Aircr. Eng. Aerosp. Tech. 79 (3) (2007) 231–237.
[31] A.C. Eringen, Mechanics of Continua, Robert E. Krieger Publishing Company, Huntington, New York, 1980.
[32] D.H. Hodges, E.H. Dowell, NASA TN D -7818, 1974.
[33] H. Du, M.K. Lim, K.M. Liew, J. Sound Vib. 175 (1994) 505–523.
[34] S.Y. Lee, Y.H. Kuo, J. Sound Vib. 162 (1993) 243–250.
[35] J.R. Banerjee, J. Sound Vib. 247 (1) (2001) 97–115.
[36] S.H.R. Eslimy-Isfahany, J.R. Banerjee, J. Sound Vib. 238 (2) (2000) 295–308.
[37] A. Bazoune, Y.A. Khulief, J. Sound Vib. 156 (1992) 141–164.
[38] Y.A. Khulief, A. Bazoune, Comput. Struct. 42 (5) (1992) 781–795.
[39] B. Downs, J. Appl. Mech. 44 (1977) 737–742.